ЛМФ 2016 (гамма-нуклон)

Лаборатория мезонной физики ОФВЭ

Отчет о ходе выполнения научно-исследовательской работы

«Барионная спектроскопия и физика с η-мезонами.

2016 г.

Сравнение результатов предсказаний моделей для числа N* and Δ–резонансов.

References	N* – resonance number	Δ – resonance number
Rev. of Part. Phys. (1980)	26	19
Rev. of Part. Phys. (2014)	19	18
KH80	21	18
KA84	18	16
CMB (Phys.Rev.D 20 1979)	16	13
T.P.Vrana et al.(nucl-th/9910012)	14	13
SM95 (Phys.Rev.C 52 1995)	13	8
FA02 (Phys.Rev.C 69, 2004)	10	7
SP06 (nucl-th/0605082)	13	9
S.Capstick et al.(Phys.Rev.D 49,1994)	40	27
U.Loring et al.(hep-ph/0103289)	99	82
Skyrme model (Phys.Rev.D31,1985)	10	13
J.Vijande et al.(hep-ph/0312165)	19	21

Экспериментальные данные по спиновой физике в гамма-протон взаимодействии на установке CB-ELSA (Бонн)

Участники от Лаборатории мезонной физики:

Д.Е. Баядилов, А.Б. Гриднев, И.В Лопатин,
Д.В. Новинский, А.К. Радьков, В.В. Сумачёв.

Ускоритель - ELectron Stretcher Anlage (ELSA)

- Energy range 0.5–3.5 GeV
- Max. extracted intensity ∼ 1nA
- Electron polarisation ∼ 60–80%

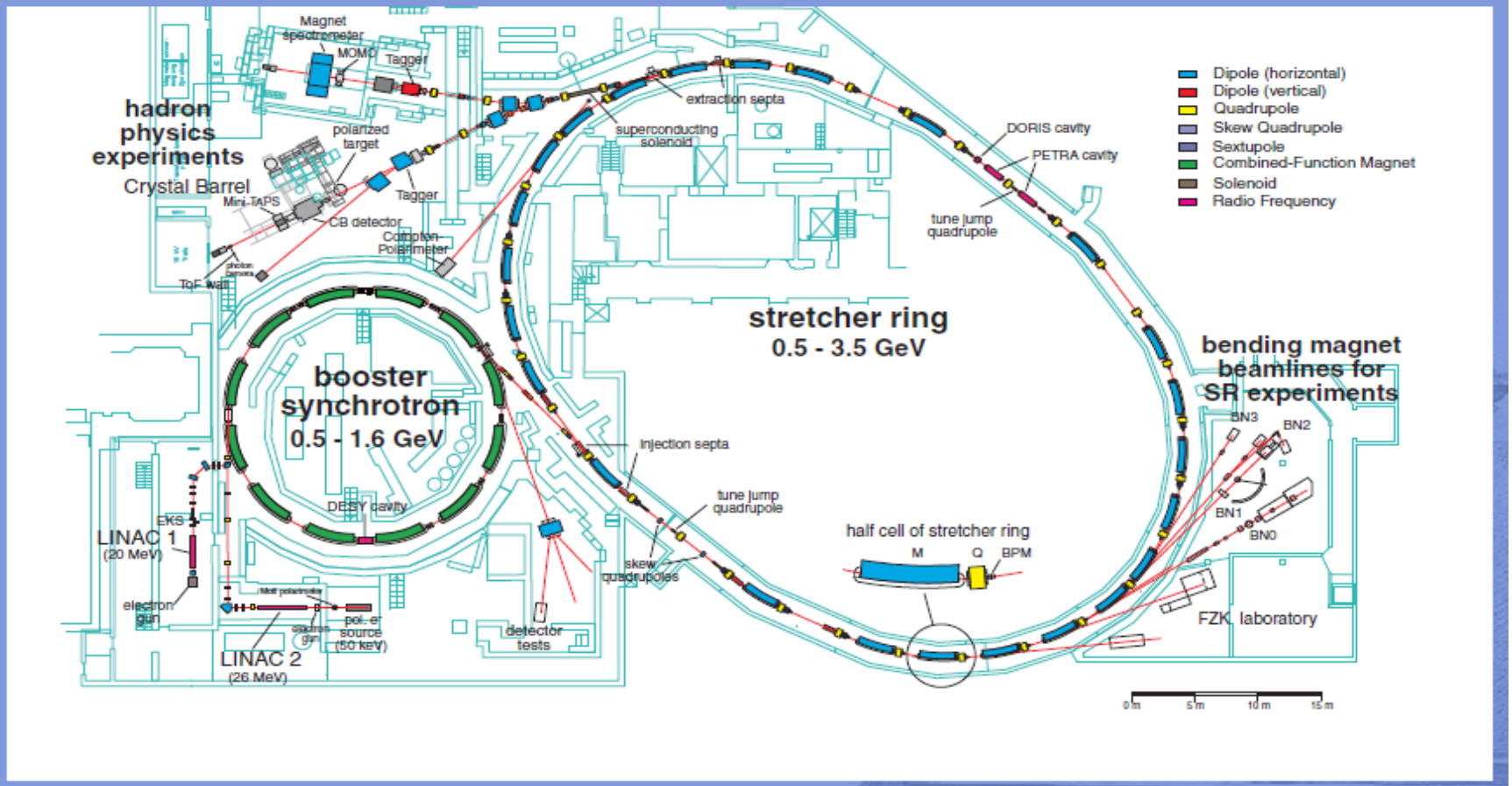

Experimental Setup

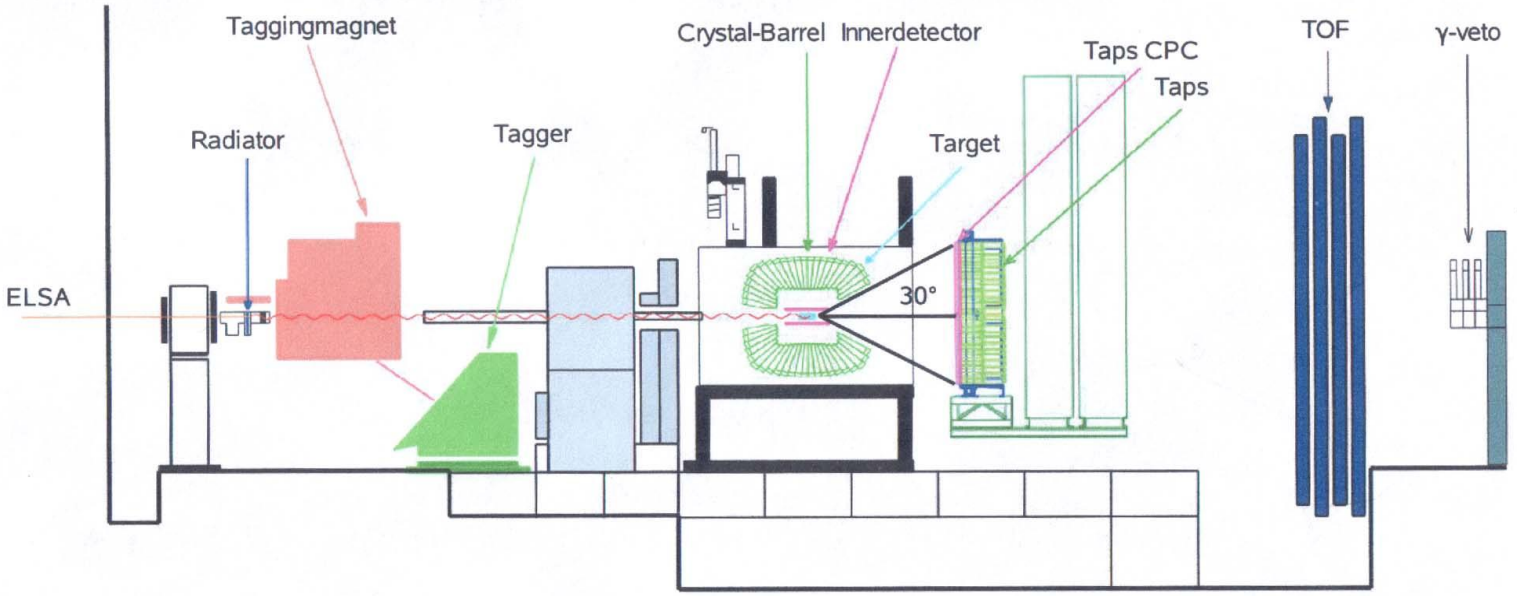

3.3 GeV $E_{electron}$ up to 3GeV photons LH_2/LD_2 1290 CsI crystals 522 BaF crystals

4π geometry, high sensitivity to multiphoton final states
physics aims:
meson production and **baryon spectroscopy**

Схема установки CB-ELSA

universitätbonn

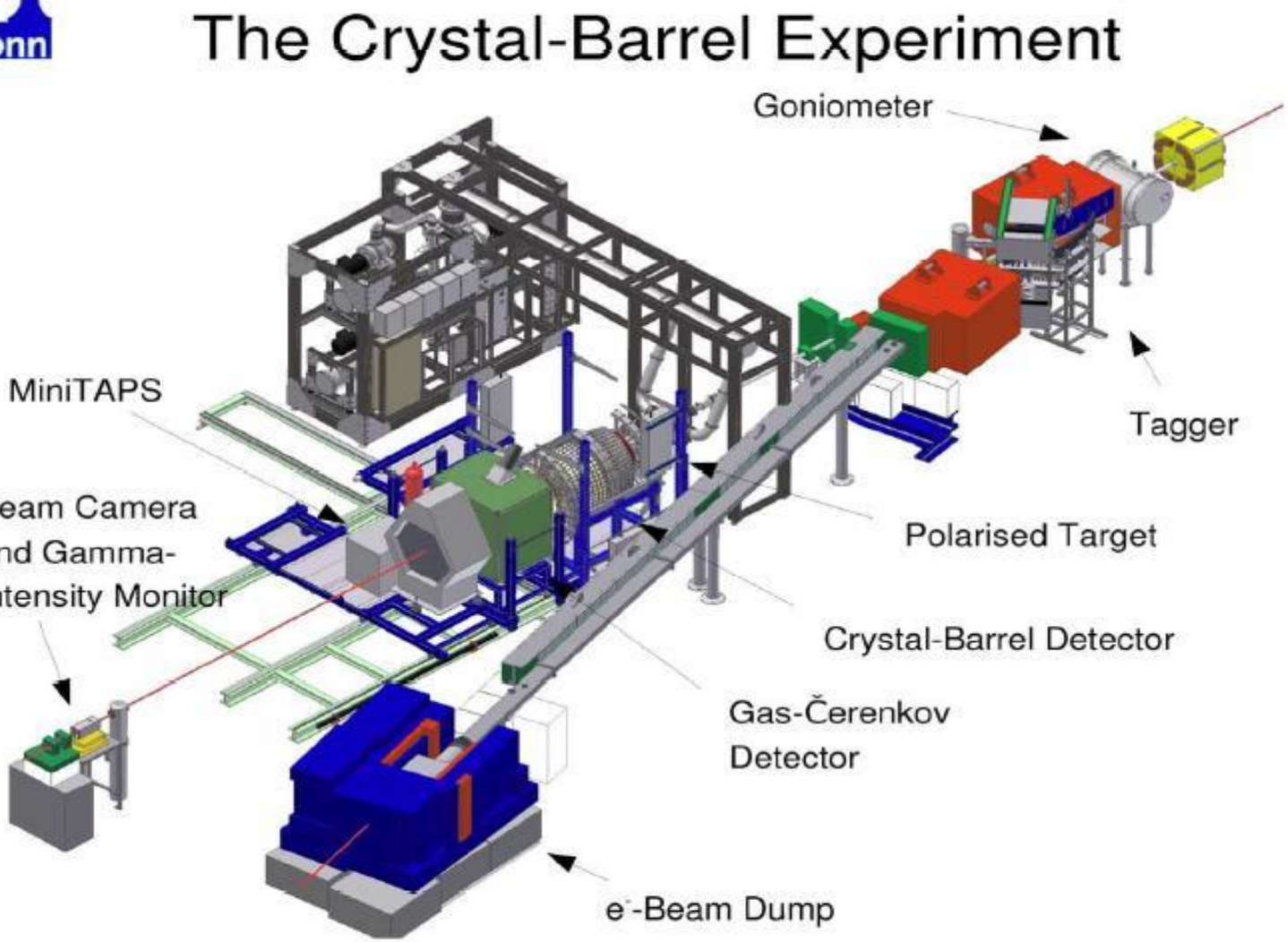

Momentum dependence of the imaginary part of the $ \omega$ - and $ \eta^{\prime}$ -nucleus optical potential.

S. Friedrich, M. Nanova, V. Metag, F.N. Afzal, D. Bayadilov, B. Bantes, R. Beck, M. Becker, S. Böse, K.T. Brinkmann, *et al.* *Показать всех 60 авторов*

Eur.Phys.J. A52 (2016) no.9, 297

Abstract.

The photoproduction of $ \omega$ and $ \eta^{\prime}$ mesons off carbon and niobium nuclei has been measured as a function of the meson momentum for incident photon energies of 1.2-2.9GeV at the electron accelerator ELSA. From the measured meson momentum distributions the momentum dependence of the transparency ratio has been determined for both mesons. Within a Glauber analysis the in-medium $ \omega$ and $\eta^{\prime}$ widths and the corresponding absorption cross sections have been deduced as a function of the meson momentum. The results are compared to recent theoretical predictions for the in-medium $ \omega$ width and $ \eta^{\prime}$ -N absorption cross sections. The energy dependence of the imaginary part of the $ \omega$ - and $\eta^{\prime}$ -Nucleus optical potential has been extracted. The finer binning of the present data compared to the existing data allows a more reliable extrapolation towards the production threshold. The modulus of the imaginary part of the $\eta^{\prime}$ -nucleus potential is found to be about three times smaller than recently determined values of the real part of the $\eta^{\prime}$ -nucleus potential, which make the $\eta^{\prime}$ meson a suitable candidate for the search for meson-nucleus bound states. For the $ \omega$ meson, the modulus of the imaginary part near threshold is comparable to the modulus of the real part of the potential. As a consequence, only broad structures can be expected, which makes the observation of $ \omega$ mesic states very difficult experimentally.

Aug 22, 2016 - 10 pages

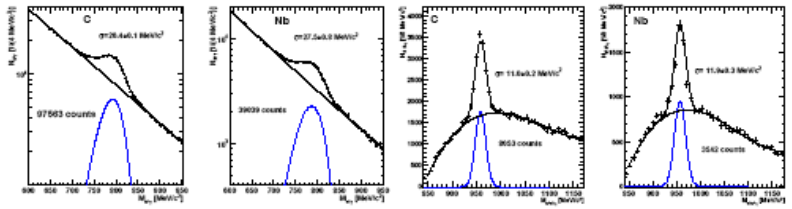

Fig. 1. (Left) $\pi^0\gamma$ and (Right) $\pi^0\pi^0\eta$ invariant mass spectra obtained for the carbon and niobium target, respectively, and for incident photon energies of 1.2-2.9 GeV. The solid lines are fits to the invariant mass spectra using a Novosibirsk- [43] (ω) and Gaussian- (η') line shape function together with an exponential (ω) or polynomial (η'), describing the background distribution. The σ values correspond to the experimental mass resolution. The plots give the number of reconstructed mesons not corrected for photon flux, detection efficiency, and decay branching ratio.

angle coverage the detector system was ideally suited for the detection and reconstruction of multi-photon events. Charged particles were registered in plastic scintillators in front of the MiniTAPS modules and the CB modules in the angular range of 11°-28°. In the polar angular range of 23°-156° charged particles were identified in a three-layer scintillating fibre array.

To improve the statistics at low ω and η' momenta the diamond radiator was used in the niobium run to generate an excess of coherent photons peaking at an energy of 1.5 GeV in addition to the $1/E_\gamma$ bremsstrahlung flux distribution. The polarisation of the radiation was not exploited in the analysis of the data. The photon flux through the target was determined by counting the photons reaching the gamma intensity monitor (GIM) at the end of the setup in coincidence with electrons registered in the tagging system. The total rate in the tagging system was ≈10 MHz. During the carbon run an aerogel-Cherenkov detector with a refractive index of n=1.05 was used to veto electrons, positrons and charged pions in the angular range covered by MiniTAPS. This device was replaced for the niobium beamtime with a gas-Cherenkov detector with a refractive index of n=1.00043 in order to veto electrons and positrons. The data were collected during two running periods of 525 h for the carbon and 960 h for the niobium target.

The ω and η' mesons were identified via the $\omega \to \pi^0\gamma \to 3\gamma$ and $\eta' \to \pi^0\pi^0\eta \to 6\gamma$ decay chains, which have a total branching ratio of 8.2% and 8.5%, respectively [38]. Events with ω and η' candidates were selected with suitable multiplicity trigger conditions. In the carbon run only events with at least four hits in the combined electromagnetic calorimeters were selected, requiring in addition that the aerogel-Cherenkov detector had not fired (veto-condition); in the niobium run a less restrictive trigger was applied, requiring two or more hits in the calorimeters and no hit in the gas-Cherenkov detector. The dead time introduced by the Cherenkov detectors were about 10% for the aerogel-Cherenkov detector and 25% for the gas-Cherenkov detector. The photon flux has been corrected for the GIM deadtime which was about 13% in the carbon run and 20% in the niobium run. A more detailed description of the detector setup and the running conditions can be found in [22,39].

3 Data analysis

Events of interest were selected and the background suppressed by several kinematical cuts. Only events with incident photon energies larger than 1.2 GeV were processed. Photons were required to have energies larger than 25 MeV to suppress cluster split off. Random coincidences between the tagger and the detector modules in the first level trigger were removed by a cut in the corresponding time spectra around the prompt peaks and a sideband subtraction.

For the ω analysis, events with three photons and one charged hit were selected. The invariant mass of all photon pairs was calculated and the one combination closest to the π^0 mass of 135 MeV/c^2 was taken to be the π^0. Events with rescattered π^0 mesons from $\omega \to \pi^0\gamma$ decays within the nucleus were suppressed by requesting the kinetic energy of the π^0 to be larger than 120 MeV [40,41]. Event losses due to this cut are taken into account in the simulation of the reconstruction efficiency (see below).The resulting $\pi^0\gamma$ invariant mass spectra for both targets are shown in Fig. 1 left.

For the η' analysis, events with only 6 photons and any number of charged hits and with an energy sum of neutral clusters larger than 600 MeV were selected. The 6 photons were combined in 2 pairs of 2 photons with invariant masses in the range 115 MeV/$c^2 \le m_{\gamma\gamma} \le$ 155 MeV/c^2 (corresponding to a $\pm 3\sigma$ cut around m_{π^0}) and one pair with invariant mass in the range 510 MeV/$c^2 \le m_{\gamma\gamma} \le$ 590 MeV/c^2 (roughly corresponding to a $\pm 2\sigma$ cut around m_η). The best photon combination was selected based on a χ^2 minimization. To suppress the background from

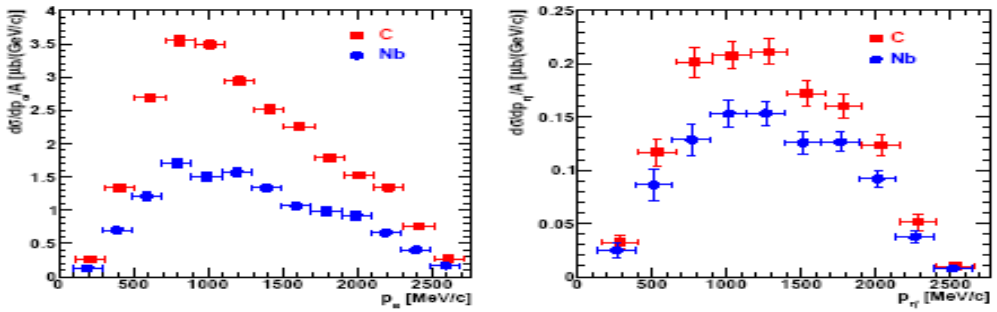

Fig. 3. Differential cross section per nucleon for (Left) ω and (Right) η' photoproduction off carbon (red squares) and niobium (blue circles) for the incident photon energies of 1.2-2.9 GeV. The data points for carbon are shifted by +10 MeV and for niobium by −10 MeV to avoid an overlap of the error bars.

shadowing [47, 48, 49] (see below) were ≈ 5%. Adding the systematic errors quadratically, the total systematic error of the cross section determinations was ≈ 17%. The determination of the transparency ratio discussed in the subsequent section requires the measurement of cross section ratios. Then, only the uncertainty for the reconstruction efficiency of the same meson in the same detector setup but for two different targets enters. This uncertainty is estimated to be reduced to 5%. The systematic uncertainty for the cross section ratio is then 20%.

Table 1. Sources of systematic errors for cross section determination.

fits	≈ 10%
reconstruction efficiency	≤10%
photon flux	5-10%
photon shadowing	≈ 5%
total	≈ 17%

4 Experimental results

Figure 3 presents the differential cross sections per nucleon for ω and η' photoproduction off carbon and niobium as a function of the meson momentum for incident photon energies of 1.2-2.9 GeV. Although the threshold for η' photoproduction off the free proton is E_γ=1.447 GeV an η' yield has been observed down to E_γ=1.2 GeV [22] due to Fermi motion, broadening, and lowering of the η' mass. Thus the momentum distributions can be determined for ω and η' mesons over the same incident photon energy range. The cross sections include a 15% correction for absorption of the incoming photon beam (photon shadowing) for both nuclear targets [47, 48, 49]. The distributions show a maximum at around 800 MeV/c and 1000 MeV/c for the ω and η', respectively, and fall off towards higher momenta. The average momenta, given in Fig. 3, are close to 1000 MeV/c. To determine the attenuation of meson m in nuclei and the inelastic meson-nucleon cross sections as a function of the meson momentum, the transparency ratio [50] is deduced from the data:

$$T_A^m = \frac{\sigma_{\gamma A\to mX}}{A\cdot\sigma_{\gamma N\to mX}}. \qquad (2)$$

The meson production cross section per nucleon within a nucleus is compared to the production cross section off a free nucleon or off a proton or neutron bound in deuterium. Here, the nucleus serves as a target and at the same time as an absorber. If nuclei were completely transparent to the mesons the transparency ratio would be unity, as long as secondary production processes can be ignored. Although the photoproduction of ω and η' mesons off protons and neutrons bound in deuterium has been studied experimentally [44, 45], differential cross sections as a function of meson momentum are not available. The momentum dependence of the transparency ratio is thus obtained by dividing the differential inclusive meson production cross sections (see Fig. 3) for niobium by the one for carbon. The transparency ratio is normalized to carbon according to

$$T_{Nb/C}^m = \frac{12\cdot\sigma_{\gamma Nb\to mX}}{93\cdot\sigma_{\gamma C\to mX}}, \qquad (3)$$

where 12 and 93 are the nuclear mass numbers of carbon and niobium, respectively. The normalization to a

Determination of the real part of the η'-Nb optical potential.

CBELSA/TAPS Collaboration
M. Nanova , S. Friedrich, V. Metag, E. Ya. Paryev, F.N. Afzal, D. Bayadilov, R. Beck, M. Becker, S. Böse, V. Crede, D. Elsner, F. Frommberger, M. Grüner, E. Gutz et al.

Phys.Rev. C94 (2016) no.2, 025205

Abstract

The excitation function and momentum distribution of η′ mesons have been measured in photoproduction off Nb93 in the energy range of 1.2–2.9 GeV. The experiment has been performed with the combined Crystal Barrel and MiniTAPS detector system, using tagged photon beams from the ELSA electron accelerator. Information on the sign and magnitude of the real part of the η′-Nb potential has been extracted from a comparison of the data with model calculations. An attractive potential of −(41±10(stat)±15(syst)) MeV depth at normal nuclear matter density is deduced within model uncertainties. This value is consistent with the potential depth of −(37±10(stat)±10(syst)) MeV obtained in an earlier measurement for a light nucleus (carbon). This relatively shallow η′-nucleus potential will make the search for η′-nucleus bound states more difficult.

Note: 9 pages, 6 figures

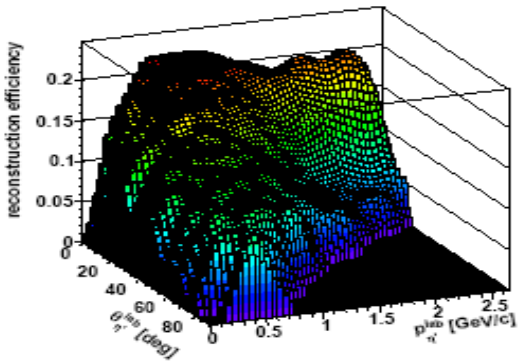

FIG. 2. (Color online) Two-dimensional reconstruction efficiency for η' photoproduction off Nb as a function of the η' momentum and laboratory angle for the incident photon energy range of 1.2-2.9 GeV.

angular resolution in the c.m. system. The statistical errors were determined from the yield of the η' signal (S) in each energy and $\cos\theta_{\eta'}^{c.m.}$ bin and the counts in the background below the peak (BG) according to the formula: $\Delta N = \sqrt{(S+BG)}$. The total cross section for η' photoproduction was determined (i) by integrating the differential cross sections and (ii) by direct determination of the η' meson yields for different incident photon energy bins. The two methods were applied as a systematic check of the fit procedure to extract the η' invariant mass signal over different kinematic ranges. The results are compared and further discussed in sec. IV B.

The different sources of systematic errors are summarised in Table I. The systematic errors in the fit procedure were estimated to be in the range of 10-15% by applying different background functions and fit intervals. Varying the start distributions in the acceptance simulation between isotropic and forward peaking η' angular distributions, the systematic errors of the acceptance determination were determined to be less than 10%. The photon flux through the target was measured by counting the photons reaching the GIM in coincidence with electrons registered in the tagger system. Systematic errors in the photon flux determination after dead time correction were estimated to be about 5-10%. The systematic errors introduced by uncertainties in the photon shadowing (see below) were ≈ 10%. The total systematic error of the cross section determinations, obtained by adding the systematic errors quadratically, was 23%.

TABLE I. Sources of systematic errors

fits	≈ 10-15%
reconstruction efficiency	≲ 10%
photon flux	5-10%
photon shadowing	≈ 10%
total	≈ 23%

IV. EXPERIMENTAL RESULTS

A. Differential cross sections for the η' photoproduction off Nb

The differential cross sections have been determined according to:

$$\frac{d\sigma}{d(\cos\theta_{\eta'}^{c.m.})} = \sum_{p_{\eta'}^{lab}} \frac{N_{\eta'\to\pi^0\pi^0\eta}(p_{\eta'}^{lab},\theta_{\eta'}^{lab})}{\epsilon_{\gamma Nb\to\eta' X}(p_{\eta'}^{lab},\theta_{\eta'}^{lab})} \cdot \frac{1}{N_\gamma \cdot n_t} \cdot \frac{1}{\Delta\cos\theta_{\eta'}^{c.m.}} \cdot \frac{1}{\frac{\Gamma_{\eta'\to\pi^0\pi^0\eta\to 6\gamma}}{\Gamma_{total}}}, \quad (4)$$

where $N_{\eta'\to\pi^0\pi^0\eta}(p_{\eta'}^{lab},\theta_{\eta'}^{lab})$ is the number of reconstructed η' mesons extracted by the fit procedure as described in Sec. III in each $(p_{\eta'}^{lab},\theta_{\eta'}^{lab})$ bin; N_γ is the photon flux; n_t is the density of the target nucleons multiplied by the target thickness $(5.55\cdot10^{21}cm^{-2})$; $\Delta\cos\theta_{\eta'}^{c.m.}$ is the angular bin in the c.m. frame; $\frac{\Gamma_{\eta'\to\pi^0\pi^0\eta\to 6\gamma}}{\Gamma_{total}}$ is the decay branching fraction of 8.5% for the decay channel $\eta'\to\pi^0\pi^0\eta\to 6\gamma$.

Fig. 3 presents the differential cross sections $d\sigma/d(\cos\theta_{\eta'}^{c.m.})$ for 8 bins in the incident photon energy range. The dead time of the gas-Cherenkov detector and the GIM have been corrected for. Furthermore, the reduction in the incident photon flux due to photon shadowing has been taken into account by multiplying the observed η' yield by 1.17 [41–43]. A rather flat angular distribution is observed at low energies near the production threshold on a free nucleon (E_γ^{thr}=1.447 GeV). For higher photon energies $E_\gamma > 1.8$ GeV, the angular distributions show a forward rise, characteristic for t-channel production. This behaviour is similar to previous results on angular distributions for η' photoproduction off carbon [22].

B. Total cross section for the η' photoproduction off Nb

The total cross section for the η' photoproduction off Nb is shown in Fig. 4 (Left). The integration of the differential cross sections and the direct determination of the cross section from the η' yield in different incident photon energy bins give consistent results within errors. The cross section is found to be non-zero below E_γ =

Double-polarization observable G in neutral-pion photoproduction off the proton.

A. Thiel, H. Eberhardt, M. Lang, F. Afzal, A.V. Anisovich, B. Bantes, D. Bayadilov, R. Beck, M. Bichow, K. -T. Brinkmann S. Böse, V. Crede, M. Dieterle, H. Dutz, D. Elsner, R. Ewald, K. Fornet-Ponse, St. Friedrich, F. Frommberger, Ch. Funke, St. Goertz, M. Gottschall, A. Gridnev, M. Grüner, E. Gutz, D. Hammann, Ch. Hammann, J. Hannappel, J. Hartmann, W. Hillert, Ph. Hoffmeister, Ch. Honisch, T. Jude, D. Kaiser, H. Kalinowsky, F. Kalischewski, S. Kammer, I. Keshelashvili, P. Klassen, V. Kleber, F. Klein, E. Klempt, K. Koop, B. Krusche, M. Kube, I. Lopatin et al.

Apr 11, 2016
e-Print: arXiv:1604.02922 [nucl-ex] | PDF

Abstract.

This paper reports on a measurement of the double-polarization observable G in π^0 photoproduction off the proton using the CBELSA/TAPS experiment at the ELSA accelerator in Bonn. The observable G is determined from reactions of linearly-polarized photons with longitudinally-polarized protons.

The polarized photons are produced by bremsstrahlung off a properly oriented diamond radiator. A frozen spin butanol target provides the polarized protons. The data cover the photon energy range from 617 to 1325 MeV and a wide angular range. The experimental results for G are compared to predictions by the Bonn-Gatchina (BnGa), J\"ulich-Bonn (J\"uBo), MAID and SAID partial wave analyses. Implications of the new data for the pion photoproduction multipoles are discussed.

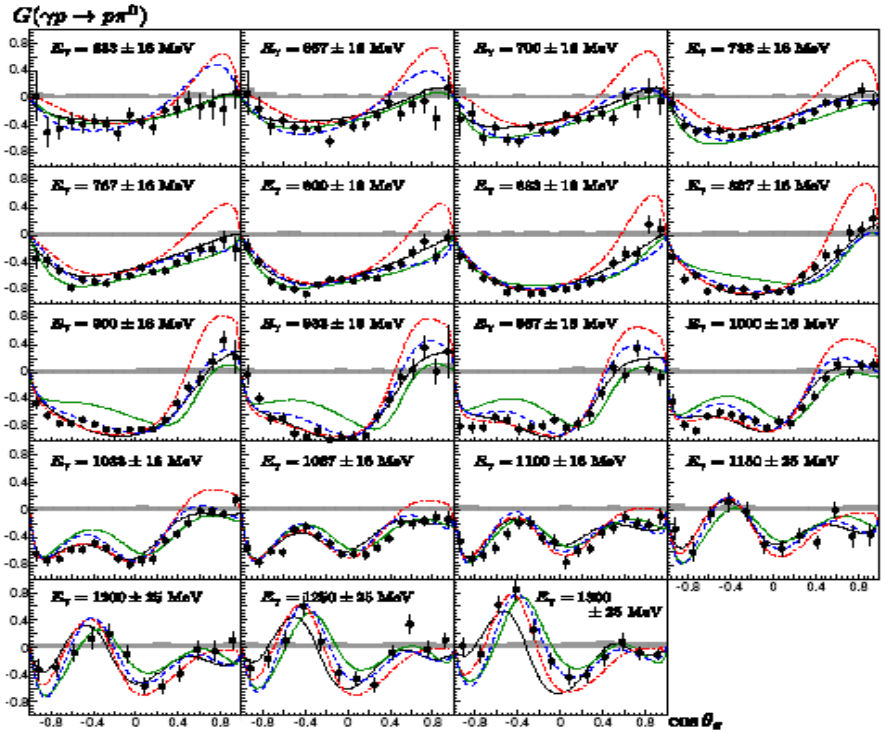

Fig. 13. The double-polarization observable G for all measured photon energies (black dots), compared to the PWA predictions: MAID 2007 [34] (green dotted line), SAID CM12 [38] (red dashed-dotted line), JüBo 2013-01 [37] (blue dashed line), and BnGa 2011-02 [39] (black solid line).

The curve represents the BnGa fit [50]. The black points demonstrate the dependence of the result on the method applied.

The left and center panel display the results for two different cut widths – 1σ and 3σ – without and with dilution-factor correction, which are called G_B and G, respectively. Of course, a proper determination of the dilution factor is decisive to obtain reliable results. However, the precise cuts used to determine G have no significant impact on the results: the center panel in Fig. 12 compares the final result using $\pm 1\sigma$ kinematical cuts with results when $\pm 3\sigma$ cuts are applied.

Finally, the double-polarization observable G can be determined in two different ways, as described in equations 3 and 7. In both cases, as shown in Figure 12 in the right panel, the different methods lead to fully consistent results. The method using Eq. 3 is used to extract the observable, since it exhibits slightly smaller errors.

Our final results are presented in Fig. 13. The figure shows the double-polarization observable G as a function of $\cos\theta_\pi$ for photon energies from $E_\gamma = 617$ MeV to $E_\gamma = 1325$ MeV. The data and the statistical errors are shown in black, the systematic errors as gray histogram. The systematic errors are derived from five sources:

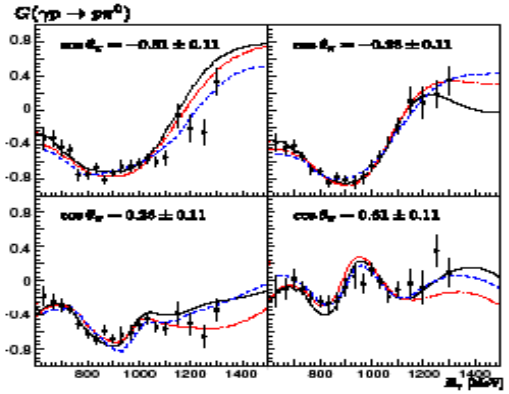

Fig. 15. The energy dependence of G for four different angles, compared to different solutions of the PWAs: BnGa 2014-02 [50] (black solid line), SAID [51] (red dashed-dotted line), and JüBo [52] (blue dashed line).

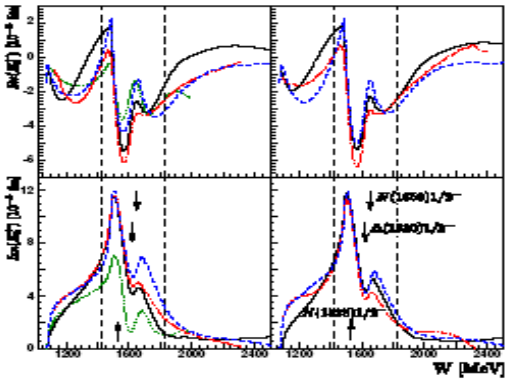

Fig. 16. The real and imaginary part of the multipole E_{0+}, before the new data were included (left) and after (right), determined by the BnGa PWA (2011-02 [39] resp. 2014-2 [50]: black solid line), the SAID (CM12 [36] resp. new fit [51]: red dashed-dotted line), the JüBo model (2015-B [37] resp. new fit [52]: blue dashed line) and the MAID model (green dotted line) [34]. The dashed lines mark the region covered by the observable G. Additionally, the positions of the resonances $N(1535)1/2^-$, $N(1650)1/2^-$ and $\Delta(1620)1/2^-$, which contribute to the E_{0+} multipole, are marked with arrows.

ment as SAID for the two lowest photon energy bins at $E_\gamma = 633$ and 667 MeV. The differences between the predictions of the MAID model and the data in the medium energy region have already been discussed in [28] and could be traced back to the multipoles E_{0+} and E_{2-}. The largest deviations between the different models can be observed in the higher energy bins ($E_\gamma > 1150$ MeV). These differences most likely occur since resonance contributions in the fourth resonance region are not well known.

The new G data were communicated to the BnGa, JüBo, and the SAID groups and new fits were performed. These are presented in Fig. 14. The new fits, BnGa 2014-02 [50] (black solid line), SAID [51] (red dashed-dotted line), and JüBo [52] (blue dashed line), reproduce the data reasonably well. Only at higher energies small deviations become visible. For convenience, we show the data in Fig. 15 for four slices in $\cos\theta$ as a function of the photon energy. All PWA fits can describe the new data very well at lower photon energies, above $E_\gamma > 1150$ MeV the fit results start to diverge. Here more precise data for G are needed to constrain the PWA solutions.

The impact of the new data can be best seen when the multipoles E_{0+}, E_{2-} and M_{2-} for the dominantly contributing resonances are compared [53]. The values of the double-polarization observable G reported here have been used as well as the data on the observables E [29], T, P, and H [30]. As an example, the real and imaginary parts of the E_{0+} multipole derived from these new fits to the data are shown in Fig. 16 and compared with the E_{0+} multipole derived from the older fits. For the imaginary part of the multipole, the spread of the solutions reduces considerably: the new data with double-polarization observables (G, E, T, P, H) have a decisive influence on the resulting multipoles. For the real part, some reduction in the spread is observed even though much less pronounced. Certainly, more data and further analyses are both required before the remaining discrepancies are resolved.

A longer paper with a comparison of all leading multipoles is in preparation [53].

4 Conclusion

The first measurement of the double-polarization observable G over a wide angular and photon energy range has been carried out with the CBELSA/TAPS experiment at the ELSA accelerator in Bonn. Simultaneously, the beam asymmetry Σ_B has been determined using a butanol target and it has been compared to the previous measurements on free protons. Small differences are attributed to bound protons in the carbon atoms of the butanol, as confirmed by a measurement on a pure carbon target.

To extract the observable G, a precise determination of the carbon contributions is necessary. With a measurement on a carbon foam target, the energy and angle-dependent dilution factor was extracted. It depends on the kinematic cuts used to extract the observable, hence the dilution factor is not a unique quantity and has to

Commissioning of the BGO-Open Dipole setup at beamline S of ELSA.

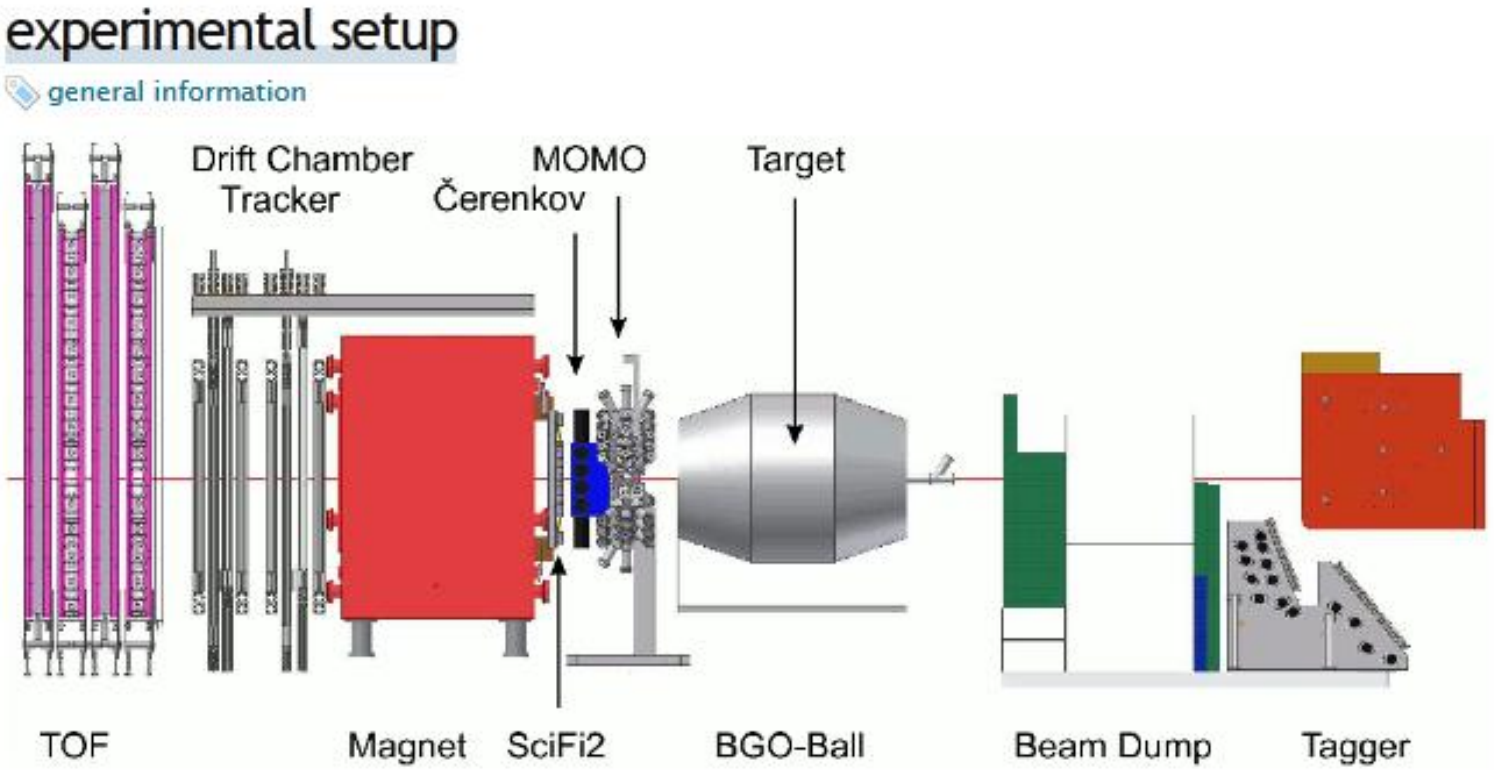

The BGO-OD experiment at ELSA

- BGO calorimeter (central region) & Forward Spectrometer combination
- High momentum resolution, excellent charged & neutral particle ID

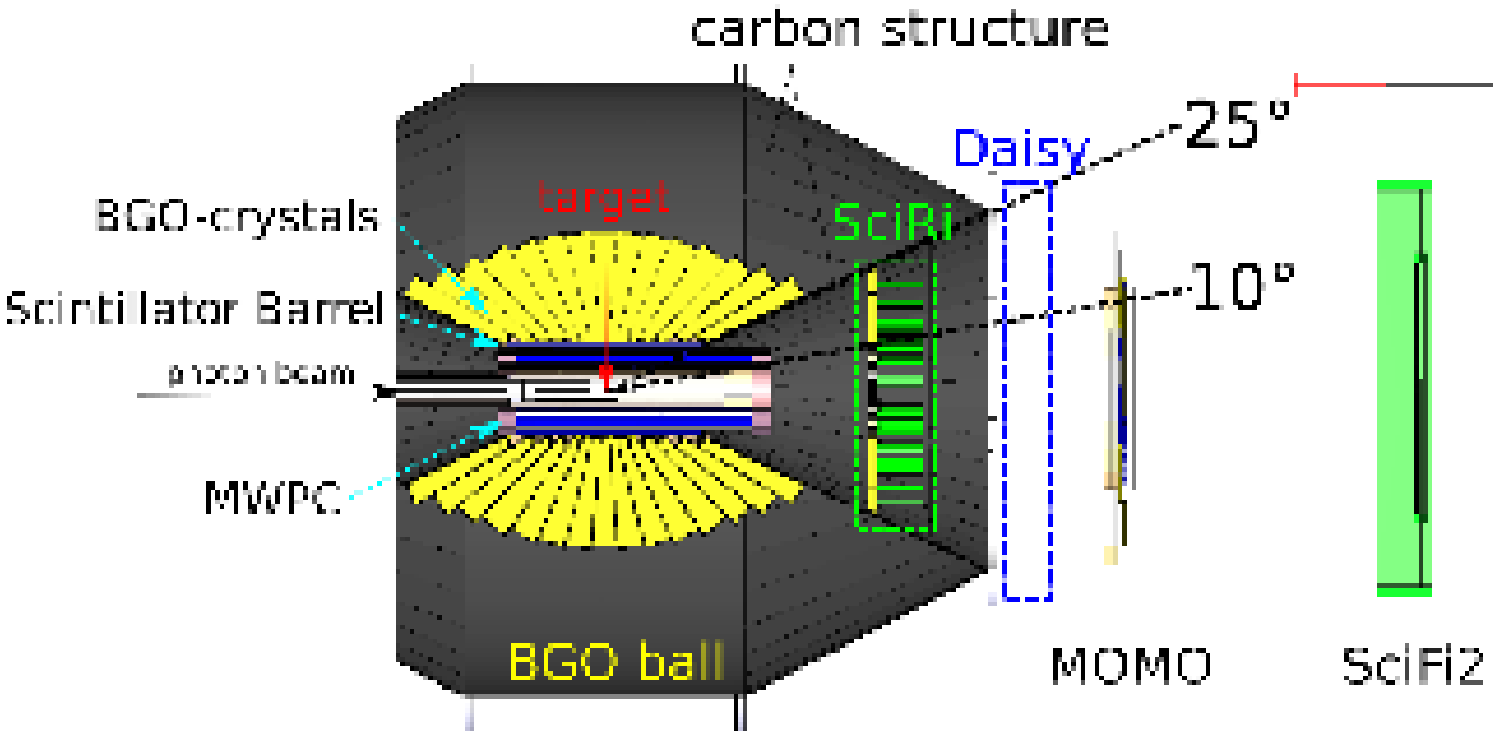

Commissioning and initial experimental program of the BGO-OD experiment at ELSA.

S. Alef, P. Bauer, **D. Bayadilov**, R. Beck, M. Becker, A. Bella, P. Bielefeldt, S. Böse , A. Braghieri, K. Brinkmann, P. Cole, R. Di Salvo, H. Dutz, D. Elsner, A. Fantini, O. Freyermuth, S. Friedrich, F. Frommberger , V. Ganenko, D. Geffers, G. Gervino, F. Ghio, S. Görtz, **A. Gridnev**, E. Gutz, D. Hammann, J. Hannappel, W. Hillert, A. Ignatov, R. Jahn, R. Joosten, T.C. Jude, F. Klein, J. Knaust, K. Kohl, K. Koop, B. Krusche, A. Lapik, P. Levi Sandri, **I.V. Lopatin**, G. Mandaglio, F. Messi, R. Messi, V. Metag, D. Moricciani, A. Mushkarenkov, M. Nanova, V. Nedorezov, **D. Novinskiy**, P. Pedroni, B. Reitz, M. Romaniuk, T. Rostomyan, N. Rudnev, C. Schaerf, G. Scheluchin, H. Schmieden, **A. Stugelev, V. Sumachev, V. Tarakanov,** V. Vegna, D. Walther, D. Watts, H. Zaunick, T. Zimmermann.

EPJ Web Conf. 130 (2016) 07013

Abstract.

BGO-OD is a new meson photoproduction experiment at the ELSA facility of Bonn University. It aims at the investigation of non strange and strange baryon excitations, and is especially designed to be able to detect weekly bound meson-baryon type structures.

The setup for the BGO-OD experiment is presented, the characteristics of the photon beam and the detector performances are shown and the initial experimental program is discussed.

2016 - 5 pages

for particle tracking and identification. The polar angles between 8° and 25° are covered by a ring of scintillating counters (*SciRi*) and by MRPC chambers (*Daisy*) with excellent time resolution. Finally, the forward region is covered by the *Open Dipole* forward spectrometer. Its central part is a 0.45 T large aperture dipole magnet (provided by DESY on permanent loan basis). Tracking is performed by position detectors in front of the magnet (*MoMo* and *Scifi2*), both consisting of scintillating fibers, and 8 double layer Drift Chambers followed by 3 ToF scintillating walls behind it.

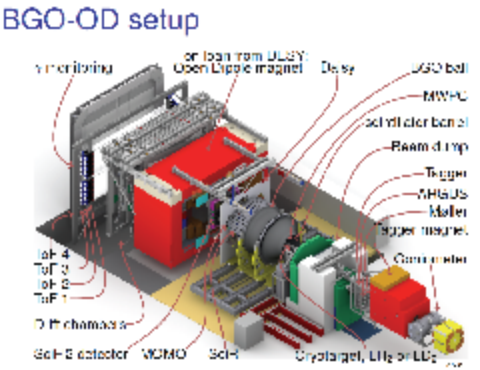

Figure 2. Schematic view of the BGO-OD experimental setup. Electron beam enters from the bottom-right corner.

The performance of the BGO *Rugby Ball* is summarized in Fig. 3 where we show the two-photon invariant mass spectrum from a proton target obtained with kinematical fit and confidence cut. The π^0, η, ω and η' peaks are all clearly visible. The energy calibration is obtained using a Na-22 source with peak at 1.275 MeV.

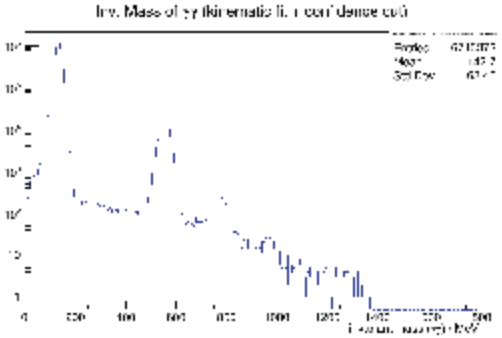

Figure 3. The two-photons invariant mass from a proton target measured by the *Rugby Ball* calorimeter.

The *Rugby Ball* can also measure protons[2] and neutrons[3], and by using sampling ADCs with ~2ns time resolution it can also measure K^+ following a method originally developed in Ref.[4]. Positive kaons are stopped within the crystals of the *Rugby Ball* up to a kinetic energy of approximately

EPJ Web of Conferences 130, 07013 (2016) DOI: 10.1051/epjconf/201613007013
MESON 2016

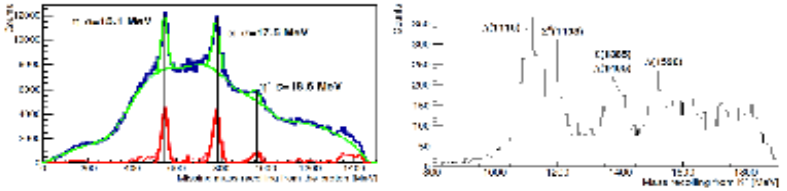

Figure 6. Missing mass spectrum in the *Open Dipole* forward spectrometer. Left: from the proton. η, ω and also η' peaks are clearly visible. Right: from the K^+. Λ and Σ^0 peaks are very clear and also other hyperons peaks are present.

CBELSA/TAPS collaboration[5] will be investigated by measuring the differential cross section in $\gamma p \rightarrow K^0\Sigma^+$ and the beam asymmetry over the K^* threshold region, achieving high statistics by including data of both neutral and charged decays of the K^0 and Σ^+. The acceptance of the *Open Dipole* forward spectrometer is also ideal to measure data at centre-of-mass angles $\theta_{cm} \leq 15°$ for K^+Y, where data are scarce and incompatible. A central goal is to disentangle the structure of hyperon excitations, e.g. the $\Lambda(1405)$ or hypothesised Σ^* states of $J^P = 1/2^-$ in the same mass range.
Pseudoscalar and vector meson photoproduction will be studied too, both off the proton and off the neutron, measuring cross sections and beam asymmetries. Thanks to the high energy resolution for the incoming photon energy provided by the *ARGUS* hodoscope, the beam asymmetry in η' photoproduction will be measured at threshold, allowing for a more detailed study of the strong energy dependence observed by the GrAAL collaboration[6], and at higher energy (up to 1800 MeV) where no experimental data are available yet. The high efficiency of the *Rugby Ball* for neutron detection will allow the measurements of η and ω off the quasi-free neutron with liquid D2 target. Finally, the Φ photoproducion will be investigated as well.

5 Conclusion

The BGO-OD experiment is commissioned; the performances of the beam and of the apparatus are as expected, production runs are underway and data analysis is ongoing for many reaction channels. The experimental program includes meson photoproduction from proton, deuteron and light nuclei.

References

[1] W. Hillert, Eur. Phys. J. A 28, 139 (2006)
[2] A. Zucchiatti *et al.*, Nucl. Instr. and Meth. A 321, 219 (1992)
[3] O. Bartalini *et al.*, Nucl. Instr. and Meth. A 562, 85 (2006)
[4] T.C. Jude, D.I. Glazier and D.P. Watts, Phys. Lett. B 735, 112 (2014)
[5] R. Ewald *et al.*, Phys. Lett. B 713, 180 (2014)
[6] P. Levi Sandri *et al.*, Eur. Phys. J. A 51, 77 (2015)

Polarized Photon Beams for the BGO-OD Experiment at ELSA.

T. Zimmermann, A. Bella, S. Alef, D. Bayadilov, R. Beck, M. Becker, P. Bielefeldt, S. Boese, A. Braghieri, K. Brinkmann P. Cole, F. Curciarello, V. De Leo, R. Di Salvo, H. Dutz, D. Elsner, A. Fantini, O. Freyermuth, S. Friedrich, F. Frommberger, V. Ganenko, G. Gervino, F. Ghio, G. Giardina, S. Goertz, A. Gridnev, E. Gutz, D. Hammann, J. Hannappel, P. Hartmann, W. Hillert, A. Ignatov, R.Jahn, R. Joosten, T.C. Jude, F. Klein, K. Koop, B. Krusche, A. Lapik, P. Levi Sandri, I.V. Lopatin, G. Mandaglio, F. Messi, R. Messi, V. Metag, D. Moricciani, A. Mushkarenkov, M.Nanova, V. Nedorezov, D. Novinskiy, P. Pedroni, B. Reitz, M. Romaniuk, T. Rostomyan, N. Rudnev, C. Schaerf, G. Scheluchin, H. Schmieden, A. Stugelev, V. Sumachev, V. Tarakanov, V. Vegna, D. Walther, D. Watts, H. Zaunick.

. **JPS Conf.Proc 10 (2016) 032003**

Abstract.

The new BGO-OD experiment at the electron accelerator ELSA, of the University of Bonn, is designed to study the reaction dynamics of nucleon excitations in meson photoproduction. It consists of a central BGO calorimeter with a magnetic spectrometer in forward direction.

The physics programme includes the measurement of polarisation observables using linearly and circularly polarised photon beams. Linear polarisation is obtained by coherent bremsstrahlung off a diamond crystal, and circular polarisation is obtained via bremsstrahlung from longitudinally polarised electrons. The degree of linear polarisation is determined from the bremsstrahlung spectrum itself. To determine the polarisation of the circularly polarised photon beam, the polarisation of the electron beam is measured by a Møller polarimeter. As a preliminary consistency check, the (linear) polarisation observable, Σ, was compared to world data for π^0 and η photoproduction. To determine the degree of circular polarisation, a Møller polarimeter was setup and first measurements of the electron beam polarisation performed.

resistive plate chamber (Daisy) and a segmented scintillator ring detector (SciRi) cover the angular region of 8°-25° between the central calorimeter and forward spectrometer.

The incident photon energy is determined using the photon tagger. The measured energy range is from 10 to 90 % of the primary electron beam energy, with a resolution of up to 0.1 %. A photon flux monitoring system is installed at the end of the beam line.

2. Linearly polarised photon beams

Linearly polarised photon beams are produced by coherent bremsstrahlung off of a 220 μm thick diamond crystal radiator [2]. This is mounted in a goniometer system to precisely align it to the beam. It is done such that the momentum transfer of the incident electron fits the reciprocal lattice and coherent bremsstrahlung is obtained. If exactly one lattice vector contributes, the momentum transfer and the bremsstrahlung plane are fixed, resulting in a well defined polarisation plane [2, 3].

A real energy spectrum is a mixture of coherent and incoherent bremsstrahlung, with the usual incoherent spectrum superimposed by enhanced peaks of coherent bremsstrahlung, as shown in fig. 2. From the intensity spectrum, it is possible to extract the degree of polarisation (fig. 3) using the Analytical Bremsstrahlung Calculation (ANB) software [4].

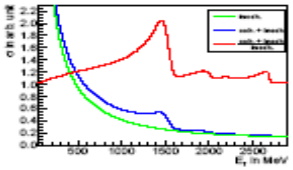

Fig. 2. Simulated bremsstrahlung intensity spectrum. Green: incoherent part. Blue: coherent part. Red: relative intensity spectrum in arb. units, i.e. blue divided by green.

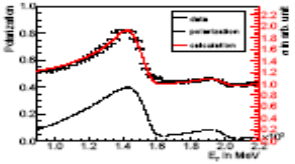

Fig. 3. Measured relative intensity spectrum. Black points: measured data in arb. units. Red solid curve: fit to the data. Black dashed curve: the resulting polarisation in parts of 1.

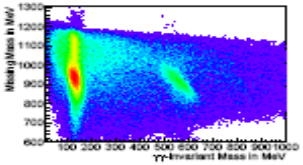

Fig. 4. The missing mass recoiling from two photons in the final state, versus the two photon invariant mass. The final states $p\pi^0$ and $p\eta$ are visible.

To perform a preliminary consistency check of our method of determining the degree of linear polarisation, the well known photon beam asymmetry, Σ, was extracted for $\gamma p \rightarrow p\pi^0$ and $\gamma p \rightarrow p\eta$ from the data of a commissioning beam time.

In the dataset used, a coherent edge was set at 1.45 GeV. A maximum polarisation of 38 % was achieved with a primary electron beam energy of 2.9 GeV.

The π^0 and η were identified by reconstructing the meson four-momentum and invariant mass from the measured energies and directions of two photons in the BGO Rugby-ball. When plotting the missing mass of the system recoiling from the meson in the final state against the two photon invariant mass, the $p\pi^0$ and the $p\eta$ reaction channels are clearly visible as peaks in fig. 4.

In figs. 5(a)-5(c), the extracted beam asymmetry is plotted against the centre of mass polar angle in one energy bin for $p\pi^0$, and two energy bins for $p\eta$. Within the limited statistical accuracy, the data is consistent with the world data, represented here by the MAID PWA solution [5]. Higher statistics over a much greater kinematic range is expected soon in the PhD thesis of Andreas Bella [6].

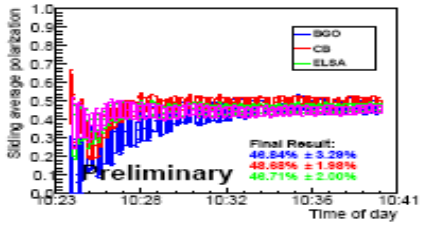

Fig. 6. Sliding average electron beam polarisation measured with two independent Møller polarimeters and different read out electronics at the CB beamline: BGO-OD (blue), CB 200 MHz Scaler (red), CB 500 MHz Scaler (green).

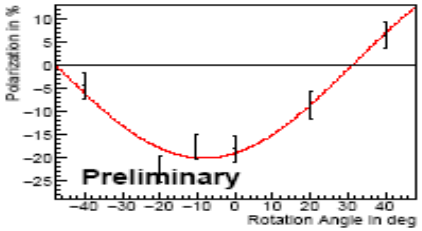

Fig. 7. Degree of circular polarisation measured at the BGO-OD beamline. Upon rotation of the electron spin at the accelerator's electron source, the data points (black) follow the expected sinusoidal behaviour (red line).

4. Conclusions and acknowledgements

The BGO-OD experiment is able to perform measurements with linearly and circularly polarised photon beams. Using a linearly polarised beam, the beam asymmetry, Σ, was extracted for $\gamma p \rightarrow p\pi^0$ and $\gamma p \rightarrow p\eta$, producing consistent results with the world data. The linear polarised beam will be used in the next production beam times.

For circularly polarisation, a Møller polarimeter was installed to measure the electron beam polarisation, and from this calculate the photon beam polarisation. This is working as expected.

This work is supported by the German Science Foundation (DFG) in the framework of the SFB/TR-16.

References

[1] W. Hillert: Eur. Phys. J. A 28 (2006) 139.
[2] U. Timm: Fortschr. Phys. 17 (1969) 765.
[3] K. Livingston: Nucl. Instrum. Methods A 603 (2009) 205.
[4] F. A. Natter *et al.*: Nucl. Instrum. Methods B 211 (2003) 465.
[5] D. Drechsel, S. S. Kamalov, and L. Tiator: Eur. Phys. J. A 34 (2007) 69.
[6] A. Bella: private communication.
[7] H. Olsen: Phys. Rev. 114 (1959) 887.
[8] C. Møller: Ann. Phys. 14 (1932) 531 [in German].
[9] H. Olsen: Springer Tr. Mod. Phys. 44 (1968) 83.
[10] S. Kammer: Dr. Thesis, Mathematisch-Naturwissenschaftlichen Fakultät, Universität Bonn, Bonn (2010).

Strangeness Photoproduction at the BGO-OD Experiment.

BGO-OD Collaboration

T.C. Jude , S. Alef, D. Bayadilov, R. Beck, M. Becker, A. Bella, P. Bielefeldt, S. Boese, A. Braghieri, K. Brinkmann, P. Cole, F. Curciarello, V. De Leo, R. Di Salvo, H. Dutz, D. Elsner, A. Fantini, O. Freyermuth, S. Friedrich, F. Frommberger, V. Ganenko, G. Gervino, F. Ghio, G. Giardina, S. Goertz, A. Gridnev, E.Gutz, D. Hammann, J. Hannappel, P. Hartmann, W. Hillert, A. Ignatov, R. Jahn, R. Joosten, F. Klein, K. Koop, B. Krusche, A. Lapik, P.Levi Sandri, I.V Lopatin, G. Mandaglio, F. Messi, R. Messi, V. Metag, D. Moricciani, A. Mushkarenkov, M. Nanova, V. Nedorezov, D. Novinskiy, P. Pedroni, B. Reitz, M. Romaniuk, T. Rostomyan, N. Rudnev, G. Scheluchin, H. Schmieden, A. Stugelev, V. Sumachev, V. Tarakanov, V. Vegna, D. Walther, D. Watts, H. Zaunick, T. Zimmermann.

JPS Conf.Proc. 10 (2016) 032002

Abstract.

BGO-OD is a newly commissioned experiment to investigate the internal structure of the nucleon, using an energy tagged bremsstrahlung photon beam at the ELSA electron facility. The setup consists of a highly segmented BGO calorimeter surrounding the target, with a particle tracking magnetic spectrometer at forward angles. BGO-OD is ideal for investigating meson photoproduction.

The extensive physics programme for open strangeness photoproduction is introduced, and preliminary analysis presented.

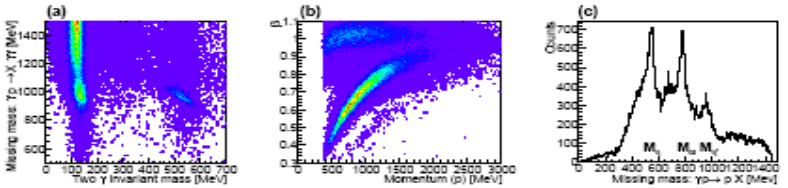

Fig. 1. (a) The missing mass, m_X, from two photons detected in BGO ball versus the invariant mass of the two photons. Peaks correspond to $p\pi^0$ and $p\eta$ final states. (b) β versus the measured momentum of charged particles in the forward spectrometer. Prominent loci of charged pions and protons are visible. (c) The missing (meson) mass from protons detected in the forward spectrometer. Meson masses labelled inset. (All analysis is preliminary and performed upon the data described in Section 4. Colour online.)

period. BGO-OD is ideal for the investigation of reactions dominated by t-channel mechanisms due to the acceptance at forward angles with high momentum resolution. Neutral particle identification in the central region aids the identification of final states of mixed charge. This unique combination is suited to the investigation of reaction channels with open strangeness and complicated final states. The first phase in this programme is the study of K^0 and K^+ reaction channels, which are described below.

Differential cross section measurements for $\gamma p \rightarrow K^0\Sigma^+$ from the CBELSA/TAPS collaboration [11] exhibited a cusp like structure close to the $K^{*+}\Lambda$ and $K^{*0}\Sigma^0$ thresholds,where the cross section reduced by a factor of four at forward angles. It was speculated that this may be due to sub-threshold production of K^* rescattering to π^0 or K^0 [12]. BGO-OD will measure the beam asymmetry, Σ, over the K^* threshold region, with high statistics by including data of both neutral and charged decays of the K^0 and Σ^+.

A paucity of data at centre of mass angles $\theta_{cm} < 15^0$ for K^+Y, prevent the constraining of isobar models [21]. The acceptance of the BGO-OD forward spectrometer is ideal to measure data at this important kinematic range. Data will also be taken over the disputed peak structure at W = 1900 MeV [22–26].

The second phase of proposals includes studies of $\gamma n \rightarrow K^0Y$. This is complementary to understand K^+Y reaction mechanisms; dominant t-channel contributions are suppressed, and hadronic coupling constants used to describe the reaction mechanisms are related via SU(3) symmetry. K^+ measurements will also be extended to search and establish higher Y^* states.

4. Preliminary analysis

The analysis presented was performed on data from the first extensive beam time period of 21 days during June and July 2015. An incident electron beam energy of 2.9 GeV was used with a liquid hydrogen target. A diamond radiator was used to produce a linearly polarised bremsstrahlung photon beam, with the coherent edge set at 1500 MeV [20]. Approximately 280 hours of data were taken with suitable hardware triggers for analysis of hadronic events.

4.1 K^+Y identification in the BGO ball

K^+ are stopped within the crystals of the BGO calorimeter up to a kinetic energy of approximately 400 MeV. Using conventional clustering algorithms, the measured energy signal is not proportional to the K^+ energy due to the subsequent weak decay within the crystals. A technique was developed

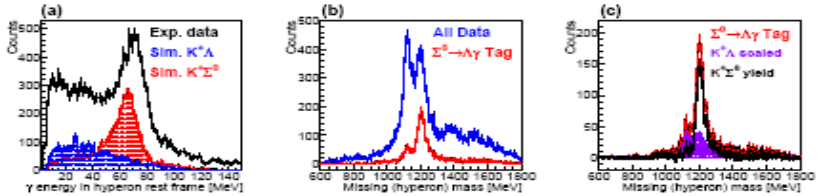

Fig. 3. (a) Photon energy after a Lorentz boost into the missing hyperon rest frame, for experimental data (black line), simulated $K^+\Lambda$ (shaded blue line) and simulated $K^+\Sigma^0$ (shaded red line). Simulated data arbitrarily scaled. (b) The missing hyperon mass from K^+ detected in the BGO for all experimental data (blue line) and events identified as $K^+\Sigma^0$ candidates (red line). (c) $K^+\Sigma^0$ candidates (red line), the efficiency scaled background from misidentified $K^+\Lambda$ candidates (shaded purple line), and the yield of $K^+\Sigma^0$ after subtraction of background (thick black line). All preliminary.

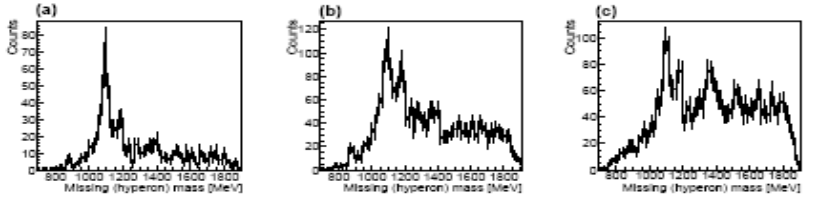

Fig. 4. The missing mass of the hyperon recoiling from the K^+ when identified in the forward spectrometer (preliminary). (a) Requiring an energy deposition less than 250 MeV and a reconstructed π^0 in the BGO ball accentuates the $K^+\Lambda$ states. (b) Requiring only an energy deposition less than 250 MeV accentuates the $K^+\Sigma^0$ and $K^+\Lambda$ final states. (c) Requiring only a reconstructed π^0 in the BGO ball accentuates higher lying Y^* states.

5. Conclusions and acknowledgements

Using commissioning data, the BGO-OD experiment and analysis is proven to be ready for studies in strangeness photoproduction. Intense data taking periods for high statistics data has begun.

We thank the technical staff of ELSA and the INFN, and the participating institutions for their invaluable contributions and acknowledge support from the Deutsche Forschungsgemeinschaft (SFB/TR16).

References

[1] R.H. Dalitz, T.C. Wong and G. Rajasekaran, Phys. Rev. 153 (1967) 1617.
[2] P.B. Siegel and W. Weise, Phys. Rev. C 38 (1988) 2221.
[3] N. Kaiser, T. Waas and W. Weise, Nucl. Phys. A 612 (1997) 297.
[4] C. Garcia-Recio, M.F.M. Lutz, and J. Nieves, Phys. Lett. B 582 (2004) 49.
[5] M.F.M. Lutz and E.E. Kolomeitsev, Phys. Lett. B 585 (2004) 243.
[6] J.C. Nacher, E. Oset, H. Toki, A. Ramos, U.G. Meissner, Nucl. Phys. A 725 (2003) 181.
[7] J.M.M Hall *et al.*, Phys. Rev. Lett. 114 (2015) 132002.

Экспериментальная установка BGO-OD идеально подходит для изучения много-частичных конечных состояний со смешанными зарядами. Надёжная идентификация частиц обеспечивается как в области малых углов, перекрываемой большим магнитным спектрометром, так и центральной области BGO-детектора. Особо следует отметить, что в переднем направлении вылета частиц высокое разрешение достигается для протонов с большими импульсами.

Кроме того, K^+- и K^--мезоны чётко идентифицируются, также одновременно, что очень важно для фоторождения φ-мезонов. Высокая эффективность регистрации нейтронов получается благодаря комбинации BGO-детектора и время-пролётного детектора. Особым достоинством является возможность использовать BGO-детектор при формировании триггера.

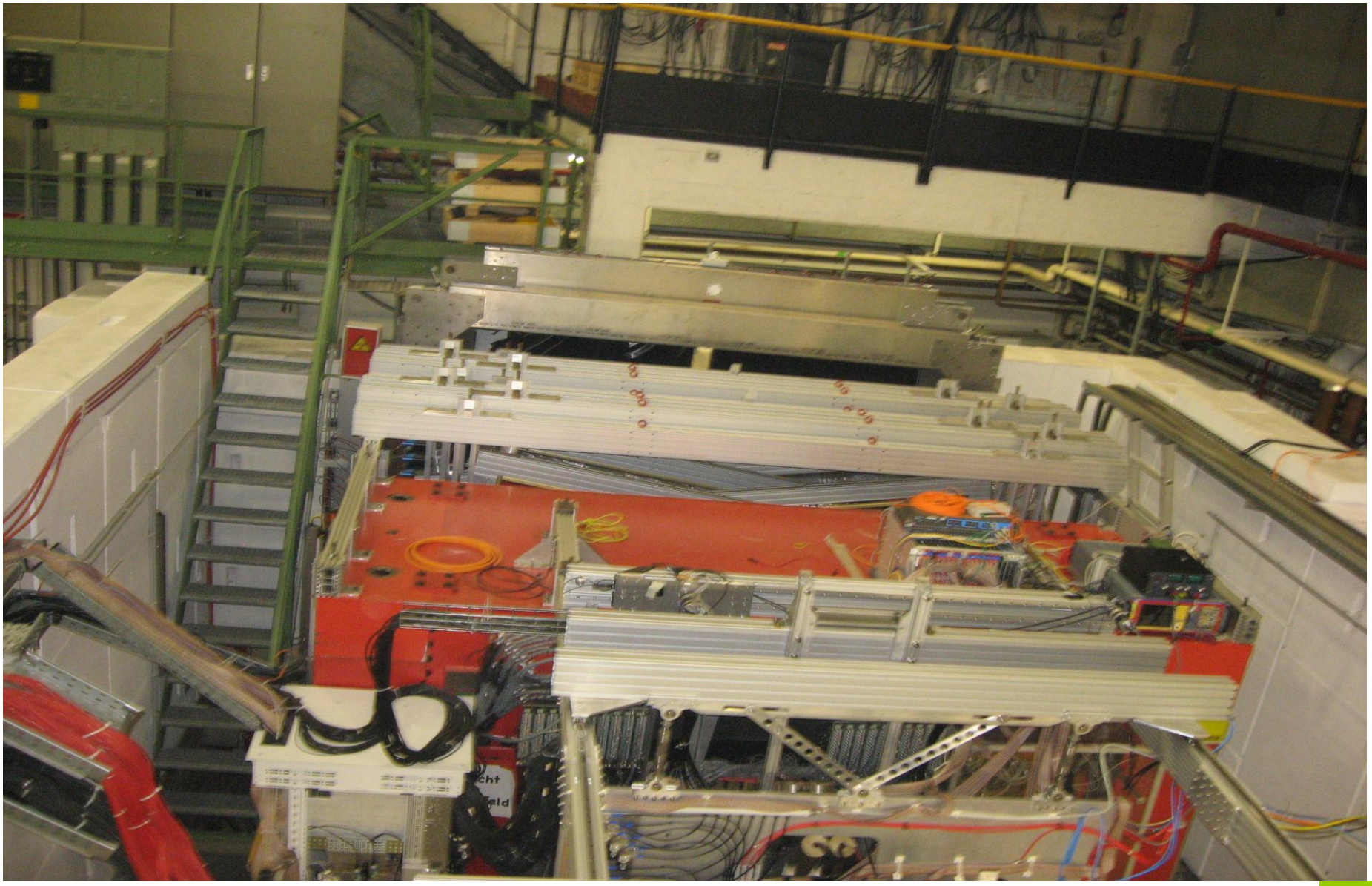

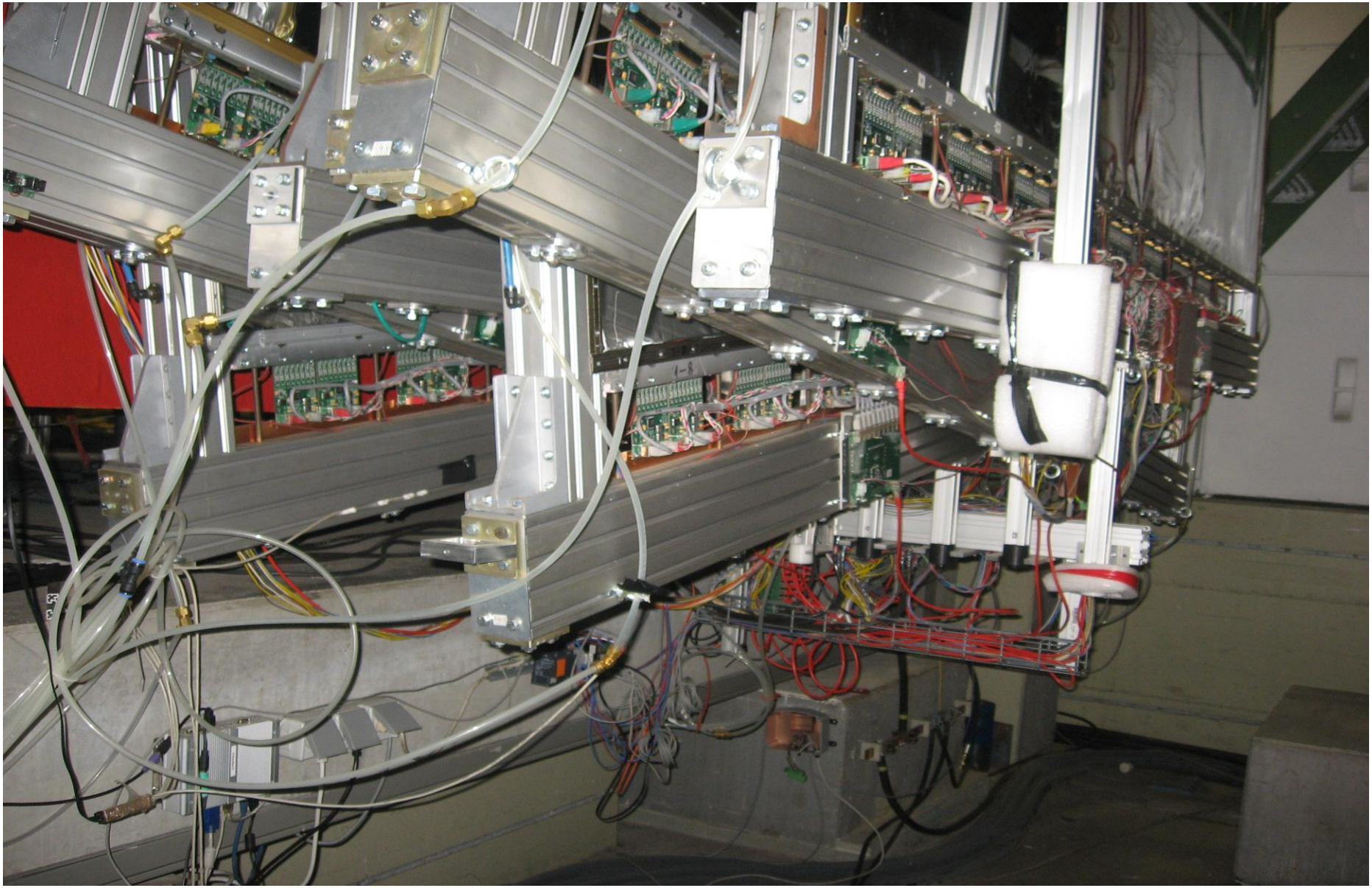

ЛМФ 2016 (гамма-нуклон)

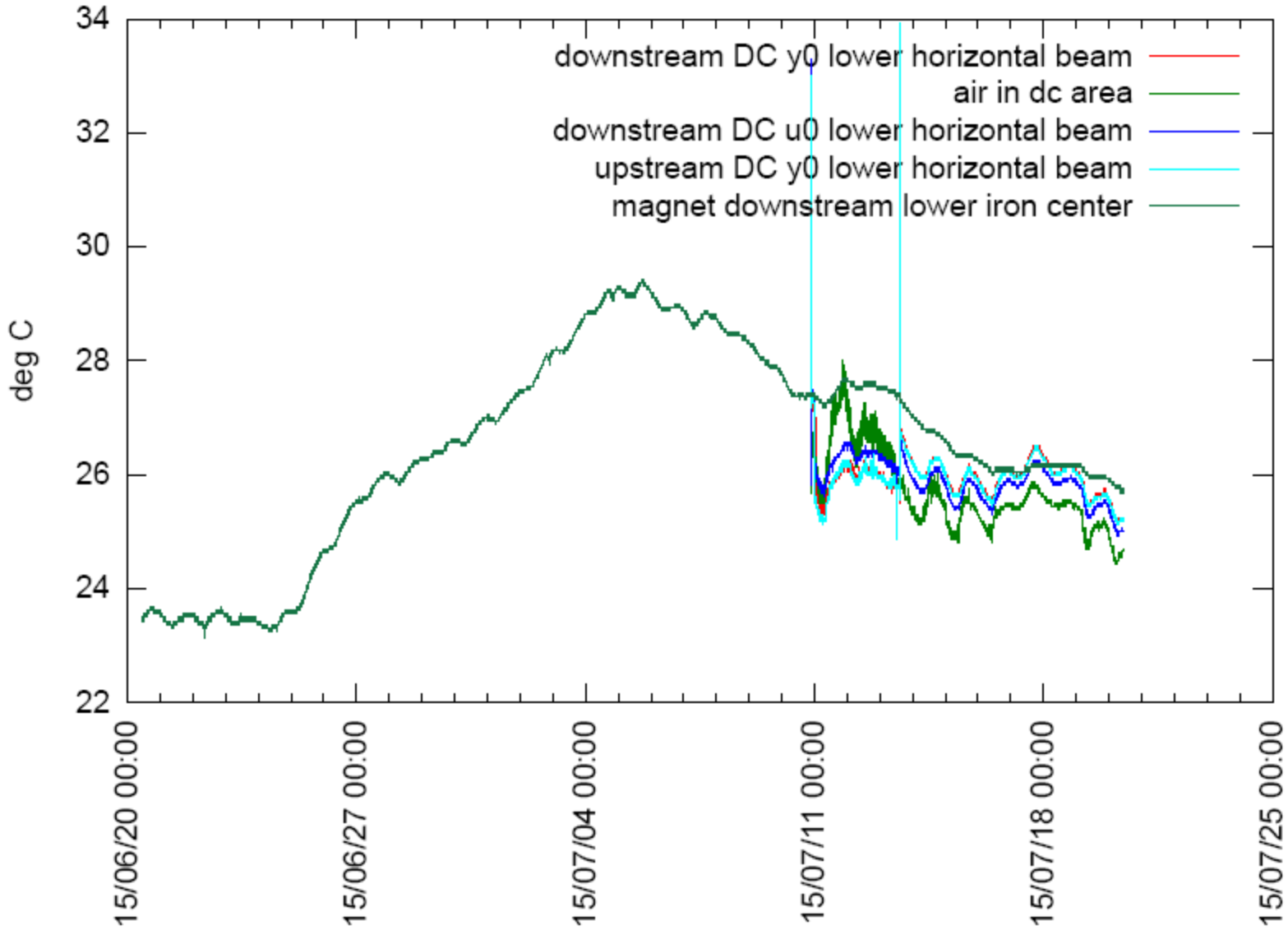

ЛМФ 2016 (гамма-нуклон)

Driftkammer - Aufbau

8 Driftkammern mit je 2 Signaldrahtebenen

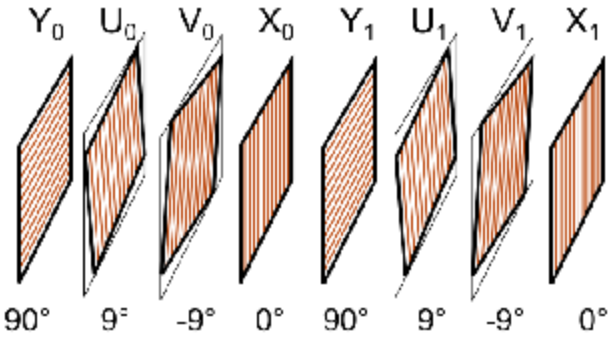

Senkrechter Schnitt durch eine Kammer

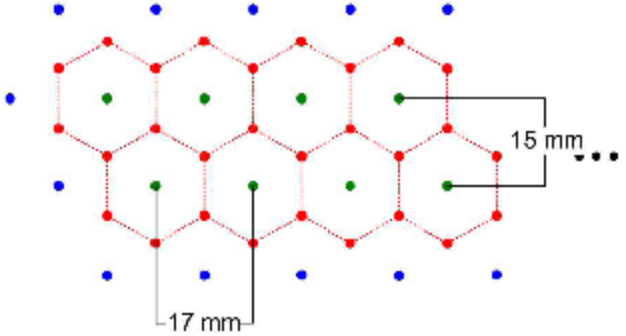

Spurrekonstruktion

Bisher:
Position der Drähte als Hit-Position

Verbesserte Rekonstruktion:
Nutze Driftzeit zur Verbesserung der räumlichen Auflösung

ЛМФ 2016 (Гамма-Нуклон)

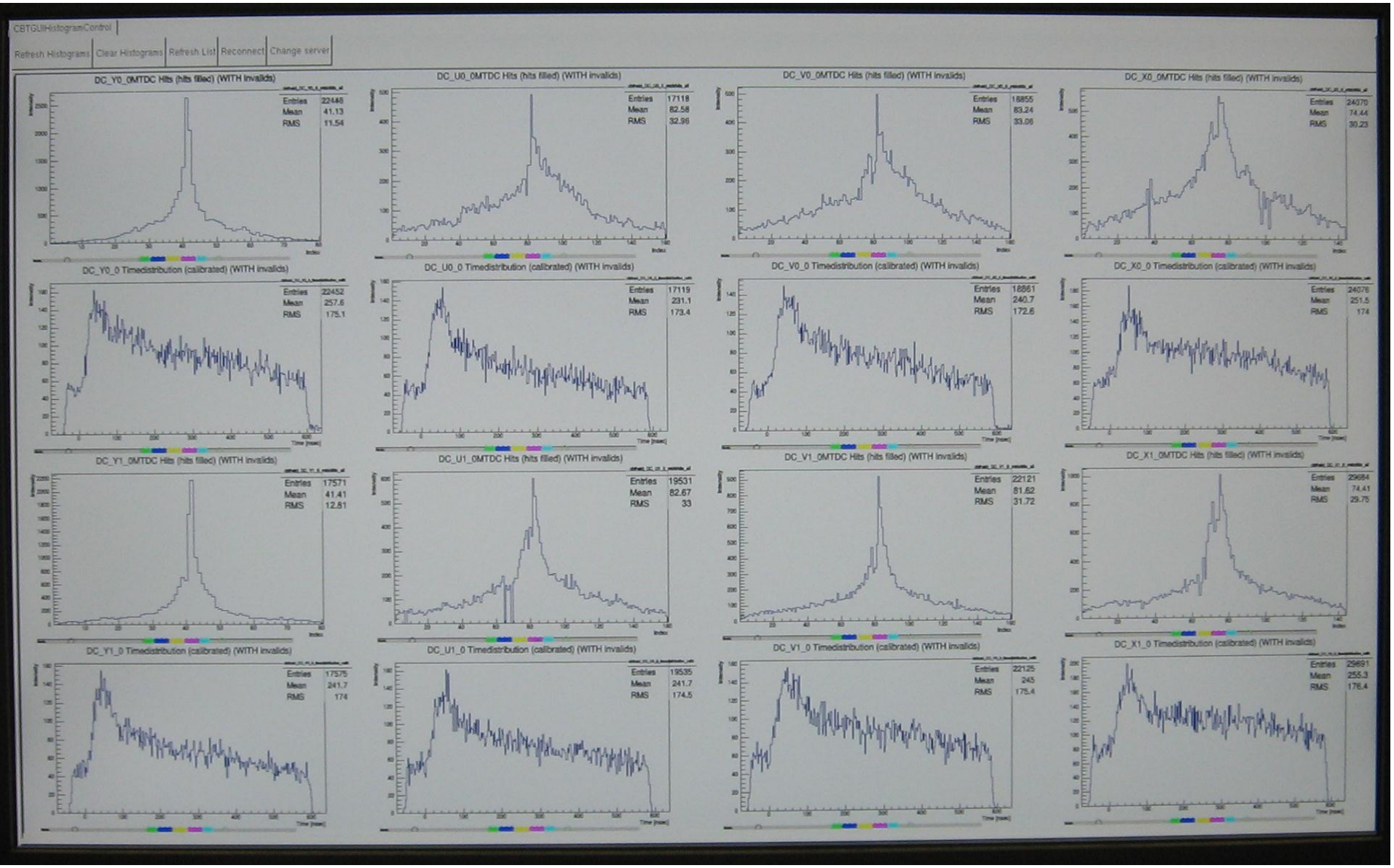

Search for narrow resonances in πp elastic scattering from the EPECUR experiment.

EPECUR Collaboration

A. B.Gridnev, I.G. Alekseev, V.A. Andreev, I.G. Bordyuzhin, W.J. Briscoe, Ye. A. Filimonov, V.V.Golubev, D.V. Kalinkin, L.I. Koroleva, N.G. Kozlenko, V.S. Kozlov, A.G. Krivshich, V.A. Kuznetsov, B.V. Morozov, V.M. Nesterov, D.V. Novinsky, V.V. Ryltsov, M. Sadler, I.I. Strakovsky, A.D. Sulimov, V.V. Sumachev, D.N. Svirida, V.I.Tarakanov, V.Yu. Trautman, R.L. Workman.

Phys.Rev. C93 (2016) no.6, 062201

Experiment: EPECUR

Abstract

The analysis of high-precision π±p→π±p cross-sectional data from the EPECUR Collaboration based on the multichannel K-matrix approach is presented. The sharp structures seen in these data are studied in terms of both opening thresholds and new resonance contributions. Some prominent features are found to be due to the opening KΣ channel. However, a complete description of the data is improved with the addition of two narrow resonant structures at W~1.686 and W~1.720GeV.

These structures are interpreted as manifestations of S11 and P11 resonances. The underlying nature of the observed phenomena is discussed.

Apr 8, 2016 - 5 pages

Планы на 2017 г.

Бонн, CB-ELSA:
Завершение модернизации установки, выход на набор статистики.

Бонн, BGO-OD:
Обеспечение надёжной работы детекторов.
Участие в циклах измерений.

Baryon resonances

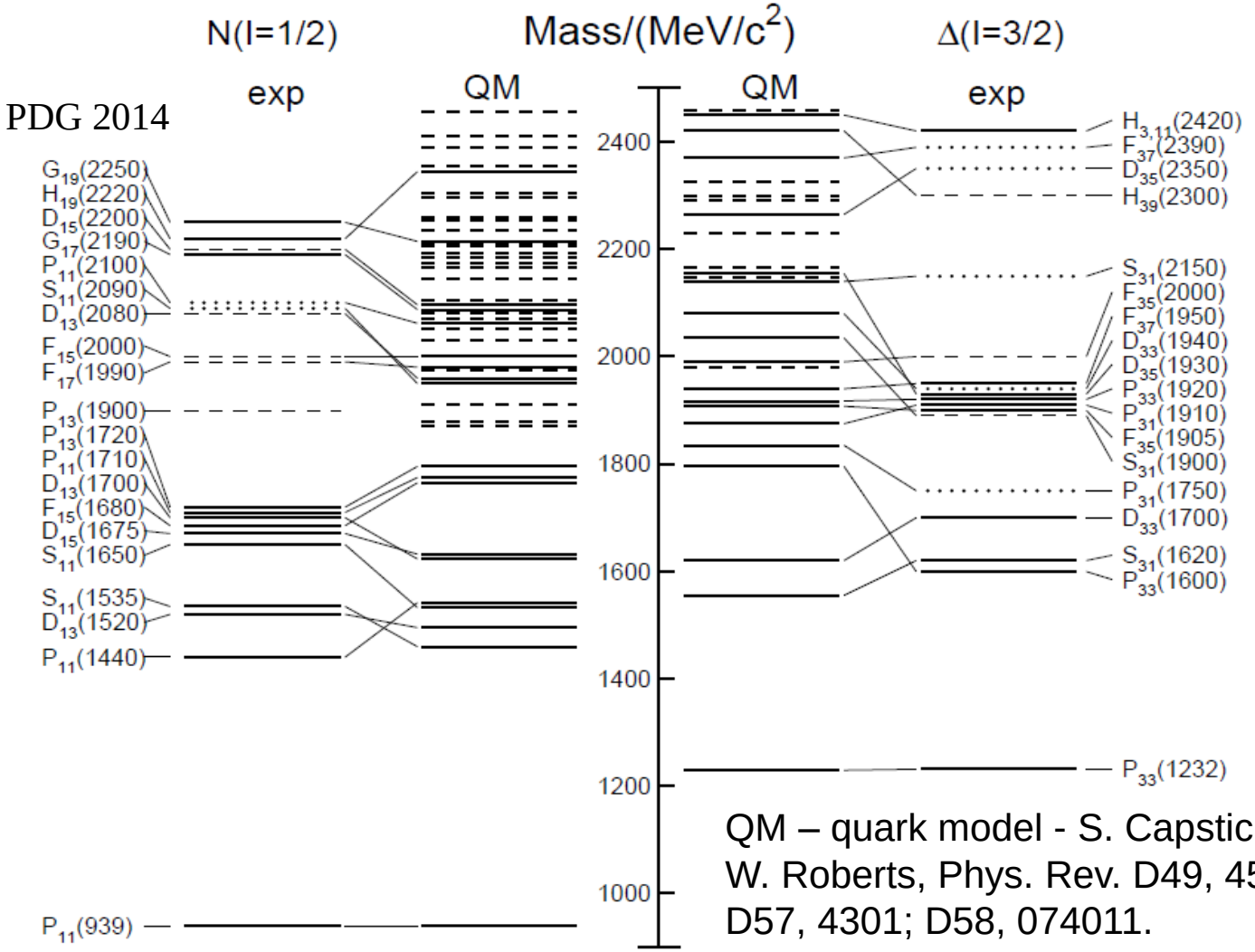

QM – quark model - S. Capstick and W. Roberts, Phys. Rev. D49, 4570; D57, 4301; D58, 074011.

Up to an excitation energy 2.4 GeV, about 45 N states are predicted but only 19 have some experimental association, including one and two-star resonaces